IEEE Access
Multidisciplinary | Rapid Review | Open Access Journal

SPECIAL SECTION ON MOBILE MULTIMEDIA FOR HEALTHCARE

Received February 21, 2019, accepted March 8, 2019, date of publication March 25, 2019, date of current version April 17, 2019.

Digital Object Identifier 10.1109/ACCESS.2019.2905875

A Novel Definition of Equivalent Uniform Dose Based on Volume Dose Curve

YIHUA LAN[1], KUN BAI[1], CHIH-CHENG HUNG[2], ABDULHAMEED ALELAIWI[3], AND ATHANASIOS V. VASILAKOS[4]

[1]School of Computer and Information Technology, Nanyang Normal University, Nanyang 473061, China
[2]Laboratory for Machine Vision and Security Research, College of Computing and Software Engineering, Kennesaw State University, Marietta, GA 30067-2896, USA
[3]Department of Software Engineering, College of Computer and Information Sciences, King Saud University, Riyadh 11543, Saudi Arabia
[4]Department of Computer Science, Electrical and Space Engineering, Luleå University of Technology, Luleå, Sweden

Corresponding author: Yihua Lan (yihualan@nynu.edu.cn)

This work was supported by the Distinguished Scientist Fellowship Program (HiCi) at King Saud University, Riyadh, Saudi Arabia.

ABSTRACT With the improvement of mobile device performance, the requirement of equivalent dose description in intensity-modulated radiation therapy is increasing in mobile multimedia for healthcare. The emergence of mobile cloud computing will provide cloud servers and storage for intensity-modulated radiotherapy (IMRT) mobile applications, thus realizing visualized radiotherapy in a real sense. Equivalent uniform dose (EUD) is a biomedical indicator based on the dose measure. In this paper, the dose volume histogram is used to describe the dose distribution of different tissues in target and nontarget regions. The traditional definition of EUD, such as the exponential form and the linear form, has only a few parameters in the model for fast calculation. However, there is no close relationship between this traditional definition and the dose volume histogram. In order to establish the consistency between the EUD and the dose volume histogram, this paper proposes a novel definition of EUD based on the volume dose curve, called VD-EUD. By using a unique organic volume weight curve, it is easy to calculate VD-EUD for different dose distributions. In definition, different weight curves are used to represent the biological effects of different organs. For the target area, we should be more careful about those voxels with a low dose (cold point); thus, the weight curve is monotonically decreasing. While for the nontarget area, the curve is monotonically increasing. Furthermore, we present the curves for parallel, serial, and mixed organs of nontarget areas separately, and we define the weight curve form with only two parameters. Medical doctors can adjust the curve interactively according to different patients and organs. We also propose a fluence map optimization model with the VD-EUD constraint, which means that the proposed EUD constraint will lead to a large feasible solution space. We compare the generalized EUD (gEUD) and the proposed VD-EUD by experiments, which show that the VD-EUD has a closer relationship with the dose volume histogram. If the biological survival probability is equivalent to the VD-EUD, the feasible solution space would be large, and the target areas can be covered. By establishing a personalized organic weight curve, medical doctors can have a unique VD-EUD for each patient. By using the flexible and adjustable EUD definition, we can establish the VD-EUD-based fluence map optimization model, which will lead to a larger solution space than the traditional dose volume constraint-based model. The VD-EUD is a new definition; thus, we need more clinical testing and verification.

INDEX TERMS Intensity modulated radiotherapy, multimedia communication, equivalent uniform dose, dose volume histogram, volume dose curve, mobile applications for health-care, mobile computing.

I. INTRODUCTION

The main difference between intensity modulated radiotherapy (IMRT) and three-dimensional conformal radiotherapy (3DCRT) is that the multileaf collimator in IMRT can modulate fluctuating intensity maps for IMRT. IMRT will radiate on the target area as much as possible as well as avoid the important nontarget tissues, which will ensure the given dose to kill cancer cells in the target area and simultaneously take care of important regions to greatly reduce radiation

The associate editor coordinating the review of this manuscript and approving it for publication was M. Shamim Hossain.

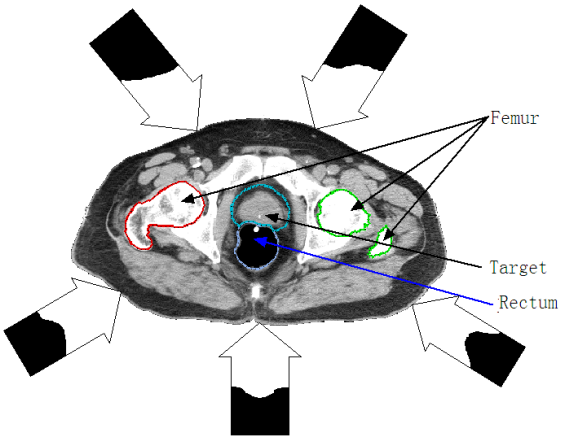

FIGURE 1. Intensity-modulated radiation field in IMRT. Five radiation fields are shown with arrows with different shapes marked with dark color. There are two types of nontarget areas, named femur and rectum, and one target.

dose [1]–[4]. Fig. 1 shows an example of intensity modulated radiation field in IMRT. As shown in Fig. 1, there are five radiation fields, and each field has different intensity-modulated radiation (represented as a different shape with dark area in five arrows). There are two types of nontarget areas, named femur and rectum, and one target outlined in Fig. 1.

Medical doctors have been trying to replace the dose satisfaction model with biomedical satisfaction models, such as the tumor control probability (TCP) and normal tissue complication probability (NTCP) models. This replacement needs an indicator for evaluation of the therapeutic effects, which is a great challenge for radiotherapy researchers [5], [6]. The equivalent uniform dose (EUD) is a kind of dose-based biomedical indicator [7], which is frequently used in the clinical system. Another kind of useful clinical evaluation system is the dose volume histogram (DVH) [8].Although the DVH can describe the clinical significance, it is not a bio-medical indicator, but physical dose indicator.

With the improvement of mobile device performance, the requirement of equivalent dose description in intensity-modulated radiation therapy is increasing in mobile multimedia for health-care [9]–[12]. The emergence of mobile cloud computing will provide cloud servers and storage for IMRT mobile applications [13]–[16].As a doctor requires that the target region dose distribution closes to the prescription dose, a minimum dose limit is often given to the target area. For the nontarget region, some of the important organ biological behavior is serial,which is called Organ at Risk (OAR). If there is any damage in any part of the organ, it will cause the entire organ to lose biological activity. Therefore, for maximum protection, doctors will give the maximum dose limit. On the contrary, in some organs, the biological behavior is parallel. Partial organ damage will not affect the normal working of the entire organ. In such a case, a doctor often gives dose volume constraints or average dose constraints.

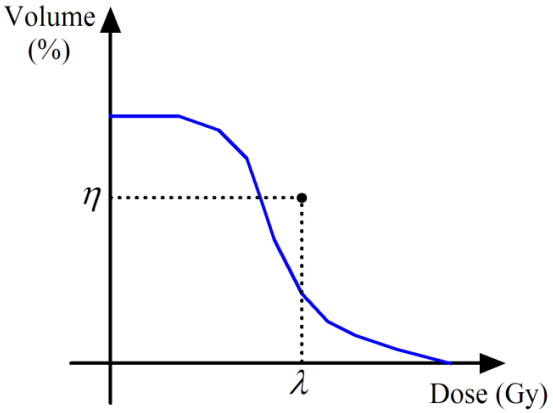

FIGURE 2. Dose volume constraints for the nontarget area. This constraint means that the dose volume curve is expected to be under the constrained point (λ, η).

Of course, there are organs that are neither serial nor parallel; consequently, the doctor will give the maximum dose limit as well as the average dose and dose volume constraints. The brain stem and spinal cord are typical serial organs. The lungs and liver are typical parallel organs. The parotid gland and rectum are neither serial nor parallel organs.

In the following sections, we will present a novel definition of equivalent uniform dose based on the volume dose curve to establish a bridge between uniform dose expression and the dose volume histogram for any kind of organ, no matter whether it is a target or nontarget region.

II. DOSE VOLUME HISTOGRAM (DVH)

A radiation oncologist often uses the dose volume histogram to describe the dose distribution in different tissues for patients in target regions and nontarget regions. For an organ at risk, the DVH plays a very important role,which can protect them. For some given tissues of an organ, the definition of DVH, $H(d)$, can be described as follows:

$$H(d) = \frac{\textit{the voxel number with receiving dose no less than } d}{\textit{the sum number of voxels}} \times 100\% \quad (1)$$

The function of the DVH is also known as the dose volume curve (DVC). Furthermore, dose volume constraints are used to control the shape characteristics of the DVC. Clinical experience shows that controlling the DVC of nontarget tissues can often play an important role in protecting organs at risk.

The dose volume constraints for a nontarget region are typically defined as no more than $\eta\%$ portion of organ voxels, which will receive λ Gy dose (or less), where Gy is an abbreviation for Gray, the international unit of radiation dose. Ideally, the dose volume constraint wants the DVC to lie below the constraint point, as shown in Fig. 2.

Similarly, dose volume constraints for the target region can be defined as no less than $\eta\%$ portion of organ voxels that will receive λ Gy dose or more. Ideally, the dose volume constraint should enforce the DVC to lie above the constrained point as shown in Fig. 3.

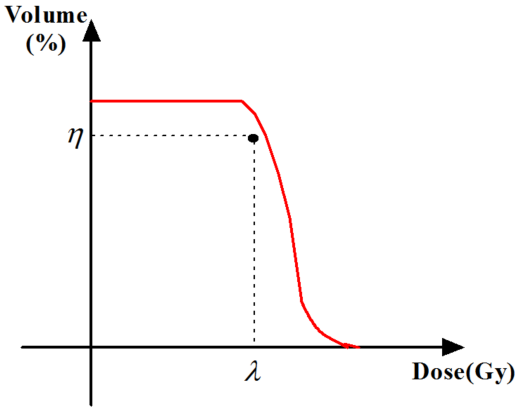

FIGURE 3. Dose volume constraints for the target area. This constraint means that the dose volume curve is expected to be above on the constrained point (λ, η).

The dose volume constraint is very important for characterizing tissue dose distribution. However, it also has higher computational complexity for inverse planning than the traditional model.

The corresponding mathematical model of the inverse planning is briefly expressed below.

Minimize quadratic functions for the penalty of target dose nonconformance Where the fluence map is variables.

S.t. Fluence map is nonnegative;

The hard constraints for target and nontarget region; and

Dose volume constraints.

III. THE TRADITIONAL EQUIVALENT UNIFORM DOSE (EUD)

The traditional equivalent uniform dose is obtained according to the Poisson distribution form [17], [18]. Assume that for a given dose D, the survival probability of a voxel can be described by an exponential function, $\exp\left(-\frac{D}{D_0}\right)$, where D_0 is the a priori value. If a prescription dose $D = 0$, it means that the voxel is not given an irradiation; i.e., $\exp\left(-\frac{D}{D_0}\right) = \exp\left(-\frac{0}{D_0}\right) = 1$, showing that the survival probability of a voxel is 100%. If a prescription dose $D = \infty$, it means that the irradiation is with a very large dose; i.e., $\exp\left(-\frac{D}{D_0}\right) = 0$, showing that the survival probability of a voxel is 0%.

Assuming that there are N voxels in an organ and that each voxel is given a dose D_i as an independent event, i is in the interval of [1, N]. We can use the following Eq. 2 to express the average survival ratio (SR) of a voxel for the event.

$$SR\left(\{D_i\}\right) = \frac{1}{N}\sum_{i=1}^{N}\exp\left(-\frac{D_i}{D_0}\right) \tag{2}$$

If we assume that all of these voxels are irradiated by the same dose (i.e., EUD), the average survival ratio can be expressed as in Eq. 3.

$$SR\left(EUD\right) = \exp\left(-\frac{EUD}{D_0}\right) \tag{3}$$

If the survival probability of voxels receiving different dosage amounts is the same as that of the same amount of doses received, it will be called equivalent uniform dose (EUD). That means $SR\left(\{D_i\}\right) = SR\left(EUD\right)$, and we have Eq. (4).

$$EUD = -D_0 \ln \frac{1}{N}\sum_{i}\exp\left(-\frac{D_i}{D_0}\right) \tag{4}$$

The generalized equivalent uniform dose (gEUD) for the target region as well as the nontarget region is obtained according to the power function as defined in Eq. (5).

$$N \cdot (gEUD)^a = \sum_{i} N \cdot w_i (D_i)^a \tag{5}$$

where w_i is the weighting parameter for voxel D_i,which represents the importance of different regions,a is a given priori value, and $\sum_i w_i = 1$. Hence, by rearranging Eq. (5), $gEUD = \left(\sum_i w_i (D_i)^a\right)^{\frac{1}{a}}$, which can be rewritten as in Eq. (6).

$$gEUD = \left(\frac{1}{N}\sum_{i} D_i^a\right)^{\frac{1}{a}} \tag{6}$$

Both the equivalent uniform dose definitions discussed above have only one presetting parameter (i.e., D_0), which is straightforward to determine. Thus, according to the formulae defined in Eqs. (4), (5) and (6), the fluence map optimization model and inverse solution methods can be used [19], [20]. In general, the EUD-based model can obtain a much larger solution space than the traditional physical dose model [21], [22]. However, the problem is that the solution obtained using a EUD-based model is often unsatisfied in the dose volume constraints [8], [23].

Although the EUD shows some useful biological meaning, the dose volume histogram (DVH) is superior in explaining the clinical significance of the dose distribution [24], [25]. On the other hand, the EUD is perfect and concise in the mathematical form, but its practical application is not necessarily related to the overall dose distributions.

Thieke proposed a linear form for the EUD [26](Eq.(7)).

$$EUD = \alpha D_{mean} + \beta D_{\max} \tag{7}$$

where parameters α and β must satisfy $\alpha + \beta = 1$,and nonnegative. $Dmean$ and $Dmax$ are the average dose and max dose of $D\,(i)$, respectively. This definition has some consistency with the power law definition to some extent. Obviously, the linear definition of the EUD provides convenient inverse fluence map modeling. However, due to its simple mathematical expression, it cannot fully meet the biomedical requirements.

IV. THE NOVEL DEFINITION

In order to maintain consistency between the EUD and DVH, we propose a novel definition of the EUD based on the volume dose curve.

To describe the volume dose curve $D(\eta\%)$ with a threshold η percentage, we sort all voxels for an organ in descending order. In contrast with the VDH, $D(\eta\%)$ represents the lower dose bound for $\eta\%$ of voxels after descending sorting, where the interval of the curve is (0, 1]. Hence, we can see that $\lim_{\eta\to 0} D(\eta\%) = D_{\max}$ and $D(100\%) = D_{\min}$.

Then, we define the corresponding weight curve $w(\eta\%)$ (increasing or decreasing) in the interval of (0, 1]. This weight curve is nonnegative in the interval with the integral $\int_0^1 w(t) = 1$.

The new EUD based on the volume dose curve (called DV_EUD) is defined as in Eq. (8).

$$DV\_EUD = \int_0^1 D(t) \cdot W(t)\, dt \tag{8}$$

In the definition, a different weight curve represents the biological effect of a different organ. For the target area, we focus on the voxels with low dose (cold voxels), and the weight curve will be monotonically increasing, as shown in Fig. 4(a). For the nontarget area, we pay more attention to the voxels with high dose (hot voxels), and the weight curve will be monotonically decreasing (Fig. 4(b)). Furthermore, for some parallel organs in the nontarget area, there is little difference in their weight for each voxel. Therefore, the weight curve can be represented by the shape of a linear curve (Fig. 4(c)). For some serial organs in the nontarget area, the hot voxels are strictly limited to protect the biological activity; thus, the curve is a steep line, which changes abruptly (Fig. 4(d)). For other mixed organs in the nontarget area, the shape of the weight curve is between the steep line and the linear line (Fig. 4(e)). The doctor can adjust the curve according to a patient's condition and type of organs. Therefore, this new definition is more flexible and adjustable.

Below, we present a weight curve definition with two parameters, b and k, where b controls the inflection point position and k controls the slope. The independent variable, t, is the volume percentage.

$$W(t) = \frac{1}{\int_0^1 \left(\arctan(k(t-b)) + \frac{\pi}{2}\right) dt} \cdot \left((\pm)\arctan(k(t-b)) + \frac{\pi}{2}\right) \tag{9}$$

The sign $(\pm)$ in Eq. (9) shows that the representation is selectable for the target or nontarget region; if the sign is positive, the weighting curve is monotonically increasing, which is applicable for the target region. On the contrary, if the sign is negative, the curve is monotonically decreasing, which is applicable for the nontarget region.

In the following, we give three examples to visualize and analyze the weighting function defined in Eq. (9). Example 1 is shown in Fig. 5; b is set to 0.5 with different k values. In example 2 (Fig. 6), k is fixed to 100 with different b values; in example 3 (Fig. 7), k is fixed to 0.01 with different b values.

Based on the results shown in Figs. 5, 6 and 7, when k is small, the change in b value has little impact on the shape of curves; this result shows that if k is close to zero (i.e., $k \to 0$), the curve represents the tissue of parallel organs. That is, the EUD of this kind organ is approaching the average dose.

When k is large, parameter b dominantly determines how many dose percentages of hot voxels were taken care of by doctors. Especially, if b is very small, the weight curve represents the tissue of serial organs. The EUD of the organs is approaching the max dose.

When k is neither very large nor small, the weight curve represents the tissue of mixed organs. The EUD corresponds to a variety of dose volume histogram, which means the proposed EUD constraint will lead to a larger feasible solution space.

A discrete version of *VD_EUD* defined in Eq. (8) is formulated in Eq. (10), where $D(i)$ is the voxel dose value and $W(i)$ is the weight of $D(i)$.

$$VD\_EUD = \sum_i D(i) \cdot W(i) \tag{10}$$

V. THE FLUENCE MAP OPTIMIZATION MODEL BASED ON THE VD-EUD

If the fluence map optimization model considers the EUD constraints, then we can formulate the model as follows: p_i is the target weight coefficient, S_{T_i} is the sum of the weights, D_{TP_i} is the prescription dose, D_{T_i} is the planning dose, EUD_j is the upper bound value for VD-EUD, and X is the fluence map variable. u represent the number of target, and v represent the number of the EUD constraints.

$$\begin{aligned} &\min \left\{ \sum_{i=1}^{u} \frac{p_i}{S_{T_i}} \left(D_{T_i} - D_{TP_i}\right)^2 \right\} \\ &S.t. \begin{cases} VD\_EUD_j \le EUD_j, \quad for\ j = 1, 2, \cdots, v \\ 0 \le X \end{cases} \end{aligned} \tag{11}$$

Its discrete version is written as shown in Eq. (12), where $Dvc_j(\bullet)$ is the dose volume value, and $D_j(\bullet)$ is the dose volume constrained upper bound, which is a nonconvex programming problem and can be solved using a heuristic algorithm [27]:

$$\begin{aligned} &\min \left\{ \sum_{i=1}^{u} \frac{p_i}{S_{T_i}} \left(D_{T_i} - D_{TP_i}\right)^2 \right\} \\ &S.t. \begin{cases} \sum_{i=0}^{1} D_j(i) \cdot W_j(i) \le EUD_j \\ Dvc_j(0) \le D_j(0) \\ Dvc_j(0.1) \le D_j(0.1) \\ \vdots \\ Dvc_j(1.0) \le D_j(1.0), \quad for\ j = 1, 2, \cdots, v \\ 0 \le X \end{cases} \end{aligned} \tag{12}$$

VI. COMPARISON AND DISCUSSION

We produce two dose distributions as the testing data in Fig. 8. These testing data will be used for the comparison of

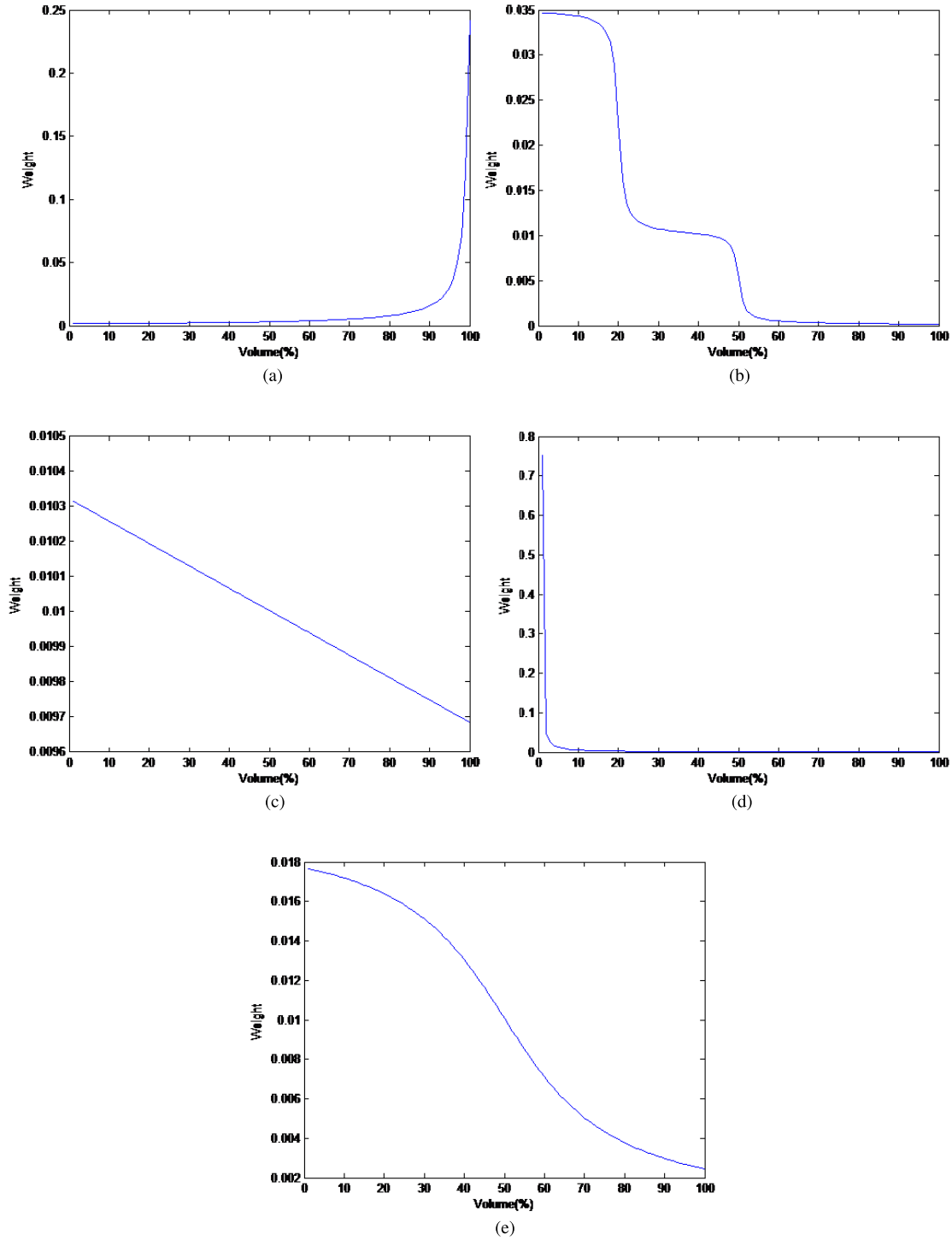

FIGURE 4. Different weight curves.

the gEUD and our proposed VD-EUD. The first dose distribution (i.e., distribution 1) is the uniform distribution from 0 Gy to 70 Gy, and the other dose distribution (i.e., distribution 2) is 2% of 70 Gy, 58% of 35 Gy, and 40% of 10 Gy. The average dose is shown in Table 1.

We compare the gEUD and the proposed VD-EUD to prove the feasibility of VD-EUD. Table 2 shows the results of gEUD based on two distributions given in Fig. 8. When parameter a is very large, gEUD represents the hot voxels. There is no significant difference between two distributions in terms of gEUD. When parameter a is equal to 1, gEUD represents the average dose of all voxels, and the difference is the largest. Overall, when parameter a is set between 1 and 100, it does not show any correlation between gEUD and the dose

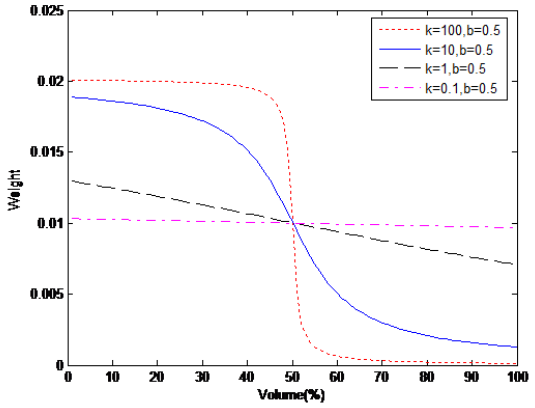

FIGURE 5. Weight curves of different combinations of k and b parameters. Parameter b is set to 0.5 with different k values.

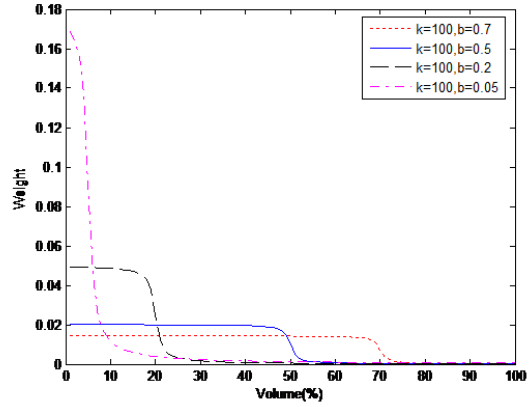

FIGURE 6. Weight curves of different combinations of k and b parameters. Parameter k is set to 100 with different b values.

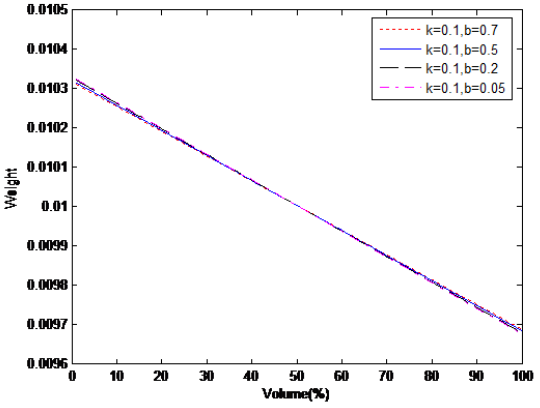

FIGURE 7. Weight curves of different parameters. Parameter k is fixed with different b values.

volume curve. In other words, it does not show that the gEUD is closely related with the dose volume curve. The change in the gEUD cannot bring about the related change in the dose volume curve. Therefore, the gEUD cannot express the difference in the dose volume curve.

In Table 3, we fix k to be 1000 and give a variety of b values from 0.02 to 1.0 to explore the relationship between VD-EUD and dose volume curve. When b is very small, the weight

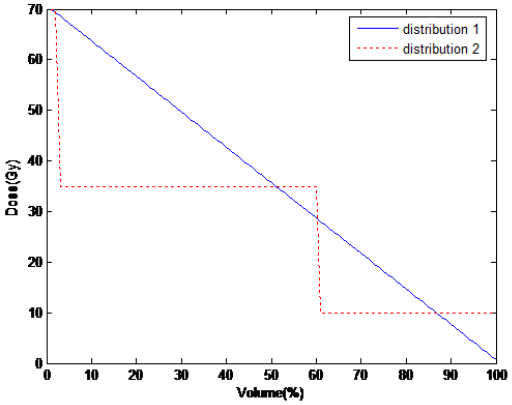

FIGURE 8. Two volume dose curves for testing dose distributions.

TABLE 1. The average dose of distributions in Fig. 8.

mean(distribution1)	mean(distribution2)	difference
35.3500	25.7000	9.6500

TABLE 2. The gEUD values of each distribution and their difference.

a*	gEUD(distribution1)	gEUD(distribution2)	difference
100	67.3145	67.1526	0.1619
50	65.0227	64.7319	0.2908
10	55.3760	47.4694	7.9066
1	35.3500	25.7000	9.6500

* a is the parameter used in formula (6).

curve focuses on the hot voxels; therefore, the difference in VD-EUD between two distributions is small. If we set b to be 1.0, the result of VD-EUD shows the average dose of all voxels; if b = 0.2, the result of weight curve shows that it is more focused on the top 20% of voxels. In this case, the VD-EUD value of distribution 1 is 63.3919, and the VD-EUD value of distribution 2 is 38.5473, which are basically the average dose of the top 20% voxels. Therefore, the VD-EUD can concentrate on any voxels and provide the most intuitive expression of dose volume histogram to doctors.Through the experiments, we can find that, the effect of b mainly represents that on which organ area the dose performance is more concerned, and the effect of k mainly represents how strict the requirement of the dose volume in a certain tissue is.

In fact, when the biological behavior of the organ is strictly serial, the VD-EUD approaches the maximum value, while the biological behavior is strictly parallel, and the VD-EUD has the mean value. Therefore, if the biological behavior of the organ is between serial and parallel, the

TABLE 3. The gEUD values of each distribution and their difference.

k and b	VD-EUD(distribution1)	VD-EUD(distribution2)	difference
k=1000, b=0.02	68.3777	66.2227	2.1550
k=1000, b=0.05	68.2429	49.9915	18.2514
k=1000, b=0.1	66.7605	42.2372	24.5233
k=1000, b=0.2	63.3919	38.5473	24.8446
k=1000, b=0.4	56.4622	36.7483	19.7139
k=1000, b=0.6	49.4907	36.1189	13.3718
k=1000, b=0.8	42.5112	29.7447	12.7665
k=1000, b=1.0	35.5596	25.7974	9.7622

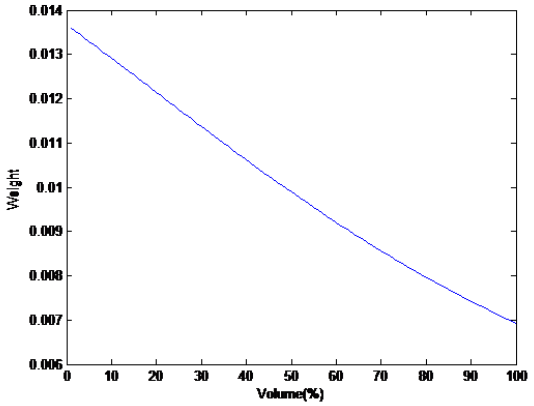

FIGURE 9. Weight curves of $k = 1$ and $b = 0.2$.

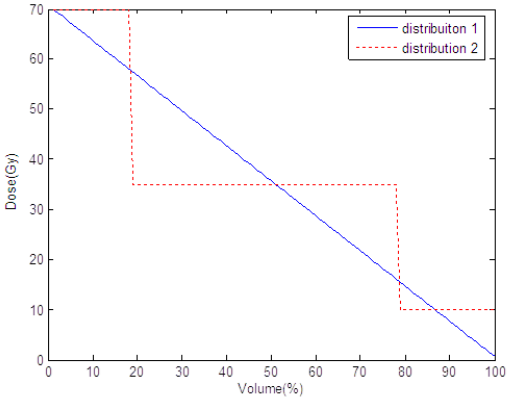

FIGURE 10. The volume dose curve of two testing dose distributions.

definition of VD-EUD will lead to a larger feasible space of dose distributions. This result shows that the unique VD-EUD can correspond to multiple dose distributions with different dose volume histograms. For example, if we set $k = 1$ and $b = 0.2$, the weight curve is suitable for the organs between serial and parallel, as shown in Fig. 9. However, the dose

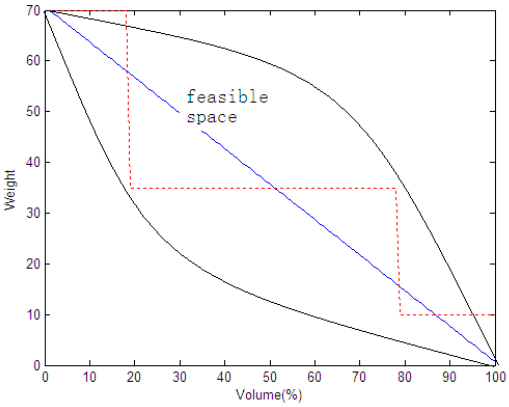

FIGURE 11. Schematic diagram of feasible space with the same VD-EUD.

volume histogram is very different, as shown in Fig. 10, and the VD-EUD of distribution 1 and distribution 2 are very similar with 39.3526 and 39.0557, respectively. From Fig. 11, for the survival probability of biological behavior to equal the uniform distribution form, the feasible space is very large. That is to say, as long as the curve is controlled within the feasible area, the dose distribution obtained can meet the clinical needs. Thus, the fluence map can consider better coverage of the target area. In the process of solving the problem, we can first give a group of dose combination vectors $D(i)$, and then select the optimal solution according to the previous quadratic programming model with dose volume constraints.

VII. CONCLUSION

The traditional definition of the equivalent uniform dose has little relationship with the dose volume histogram, and this paper proposed a novel volume dose curve-based equivalent uniform dose (VD-EUD). Through the establishment of personalized organic weight curve, doctors can provide patients with the equivalent uniform dose more precisely using the proposed VD-EUD. With VD-EUD, we can establish a new EUD-based fluence map optimization model, which leads to a larger solution space than the traditional DVC-based model and still maintain the significance of biological behavior. The next step of research will be to apply it to clinical practice.

REFERENCES

[1] B. Rigaud *et al.*, "CBCT-guided evolutive library for cervical adaptive IMRT," *Med. Phys.*, vol. 45, no. 4, pp. 1379–1390, Apr. 2018.
[2] B. Wu, D. Pang, P. Simari, R. Taylor, G. Sanguineti, and T. Mcnutt, "Using overlap volume histogram and IMRT plan data to guide and automate VMAT planning: A head-and-neck case study," *Med. Phys.*, vol. 40, no. 2, 2016, Art. no. 021714.
[3] R. Townson, H. Egglestone, and S. Zavgorodni, "A fast jaw-tracking model for VMAT and IMRT Monte Carlo simulations," *J. Appl. Clin. Med. Phys.*, vol. 19, no. 4, pp. 26–34, 2018.
[4] D. J. Sher, R. B. Tishler, N. L. Pham, and R. S. Punglia, "Cost-effectiveness analysis of intensity modulated radiation therapy versus Proton therapy for oropharyngeal squamous cell carcinoma," *Int. J. Radiat. Oncol. Biol. Phys.*, vol. 101, no. 4, pp. 875–882, Jul. 2018.
[5] D. M. Aleman, H. E. Romeijn, and J. F. Dempsey, "A response surface approach to beam orientation optimization in intensity-modulated radiation therapy treatment planning," *Informs J. Comput.*, vol. 21, no. 1, pp. 62–76, 2017.

[6] J. Olasolo-Alonso, A. Vázquez-Galiñanes, S. Pellejero-Pellejero, J. F. Pérez-Azorín, "Evaluation of MLC performance in VMAT and dynamic IMRT by log file analysis," *Phys. Medica*, vol. 33, pp. 87–94, Jan. 2017.
[7] J. Zhu *et al.*, "The benefit of using bladder sub-volume equivalent uniform dose constraints in prostate intensity-modulated radiotherapy planning," *Onco Targets Therapy*, vol. 9, pp. 7537–7544, Dec. 2016.
[8] K. Senthilkumar, K. J. M. Das, K. Balasubramanian, A. C. Deka, and B. R. Patil, "Estimation of the effects of normal tissue sparing using equivalent uniform dose-based optimization," *J. Med. Phys.*, vol. 41, no. 2, pp. 123–128, Apr./Jun. 2016.
[9] Y. Zhang, R. Gravina, H. Lu, M. Villari, and G. Fortino, "Pea: Parallel electrocardiogram-based authentication for smart healthcare systems," *J. Netw. Comput. Appl.*, vol. 117, pp. 10–16, Sep. 2018.
[10] M. S. Hossain, G. Muhammad, and A. Alamri, "Smart healthcare monitoring: A voice pathology detection paradigm for smart cities" in *Proc. Multimedia Syst.*, pp. 1–11, Jul. 2017.
[11] Y. Hu, K. Duan, Y. Zhang, M. S. Hossain, S. M. M. Rahman, and A. Alelaiwi, "Simultaneously aided diagnosis model for outpatient departments via healthcare big data analytics," *Multimedia Tools Appl.*, vol. 77, no. 3, pp. 3729–3743, 2018.
[12] M. Chen, J. Yang, L. Hu, M. S. Hossain, and G. Muhammad, "Urban healthcare big data system based on crowdsourced and cloud-based air quality indicators," *IEEE Commun. Mag.*, vol. 56, no. 11, pp. 14–20, Nov. 2018. Accessed: Feb. 27, 2019. doi: 10.1109/MCOM.2018.1700571.
[13] M. S. Hossain, "Cloud-supported cyber–physical localization framework for patients monitoring," *IEEE Syst. J.*, vol. 11, no. 1, pp. 118–127, Mar. 2017.
[14] Y. Qian, Y. Zhang, Y. Ma, H. Yu, and L. Peng, "EARS: Emotion-aware recommender system based on hybrid information fusion," *Inf. Fusion*, vol. 46, pp. 141–146, Mar. 2019.
[15] M. S. Hossain, "Patient state recognition system for healthcare using speech and facial expressions," *J. Med. Syst.*, vol. 40, no. 12, p. 272, Dec. 2016.
[16] Y. Zhang, Y. Qian, D. Wu, M. S. Hossain, A. Ghoneim, and M. Chen, "Emotion-aware multimedia systems security," *IEEE Trans. Multimedia*, vol. 21, no. 3, pp. 617–624, Mar. 2019.
[17] P. S. Potrebko, J. Fiege, M. Biagioli, and J. Poleszczuk, "Investigating multi-objective fluence and beam orientation IMRT optimization," *Phys. Med. Biol.*, vol. 62, no. 13, pp. 5228–5244, Jul. 2017.
[18] M. Hussein *et al.*, "Clinical validation and benchmarking of knowledge-based IMRT and Vmat treatment planning in pelvic anatomy," *Radiotherapy Oncol.*, vol. 120, no. 3, pp. 473–479, Sep. 2016.
[19] W. P. Smith, M. Kim, C. Holdsworth, J. Liao, and M. H. Phillips, "Personalized treatment planning with a model of radiation therapy outcomes for use in multiobjective optimization of IMRT plans for prostate cancer," *Radiat. Oncol.*, vol. 11, no. 1, pp. 1–14, 2016.
[20] G. Liu and J. Liu, "SU-F-T-335: Piecewise uniform dose prescription and optimization based on PET/CT images," *Med. Phys.*, vol. 43, no. 6, p. 3540, Jun. 2016.
[21] A. Youssoufi, M. Bougtib, M. E. Baraka, M. Erraoudi, and F. Bentayeb, "Optimization of IMRT techniques for two dose levels irradiation of larynx cancer," *Phys. Medica*, vol. 32, no. 3, p. 262, Sep. 2016.
[22] S. Zieminski, M. Khandekar, and Y. Wang, "Assessment of multi-criteria optimization (MCO) for volumetric modulated arc therapy (VMAT) in hippocampal avoidance whole brain radiation therapy (HA-WBRT)," *J. Appl. Clin. Med. Phys.*, vol. 19, no. 2, pp. 184–190, Mar. 2018.
[23] P. Kukolowicz and M. Mrozowska, "Ep-1552: What dose distribution metrics in the PTV can be used instead of the generalized equivalent uniform dose?" *Radiotherapy Oncol.*, vol. 111, no. 7, pp. S184–S185, Jan. 2014.
[24] A. Fogliata, S. Thompson, A. Stravato, S. Tomatis, M. Scorsetti, and L. Cozzi, "On the gEUD biological optimization objective for organs at risk in photon optimizer of eclipse treatment planning system," *J. Appl. Clin. Med. Phys.*, vol. 19, no. 1, pp. 106–114, Jan. 2018.
[25] H. Mescher, S. Ulrich, and M. Bangert, "Coverage-based constraints for IMRT optimization," *Phys. Med. Biol.*, vol. 62, no. 18, p. N460, Sep. 2017.
[26] T. Long, M. Chen, S. Jiang, and W. Lu, "Continuous leaf optimization for IMRT leaf sequencing," *Med. Phys.*, vol. 43, no. 10, pp. 5403–5411, Oct. 2016.
[27] Y. Lan, C. Li, H. Ren, Y. Zhang, and Z. Min, "Fluence map optimization (FMO) with dose-volume constraints in IMRT using the geometric distance sorting method," *Phys. Med. Biol.*, vol. 57, no. 20, pp. 6407–6428, Sep. 2012.

YIHUA LAN received the Ph.D. degree in computer science and technology from the Huazhong University of Science and Technology (HUST), in 2011, where he was a Postdoctoral Fellow with the School of Computer Science and Technology, for four years from 2013. He is currently an Associate Professor of computer science with the School of Computer and Information Technology, Nanyang Normal University, China, where he also holds the position of WoLong Scholar. His main research interests include cloud computing, machine learning, and computer-aided diagnosis.

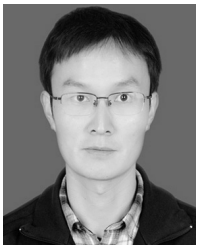

KUN BAI received the Ph.D. degree in computer science from Dalian Maritime University, China, in 2012. He is currently a Lecturer with Nanyang Normal University. His research interests include optimization algorithm and machine learning.

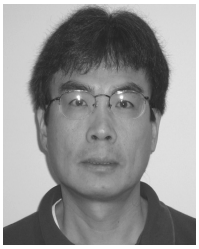

CHIH-CHENG HUNG received the B.S. degree in business mathematics from Soochow University, Taiwan, and the M.S. and Ph.D. degrees in computer science from the University of Alabama, Huntsville, AL, USA, in 1986 and 1990, respectively. He is currently a Professor of computer science with Kennesaw State University (KSU), USA, where he is the Director of the Center for Machine Vision and Security Research. He also holds the position of YinDu Scholar with National Anyang University, Anyang, China. He will be serving as the Conference Chair for the Association of Computing Machinery (ACM) Symposium on Applied Computing (SAC 2019) to be held in Limassol, Cyprus, in 2019. His research interests include image processing, pattern recognition, machine learning, neural networks, genetic algorithms, and artificial intelligence.

ABDULHAMEED ALELAIWI received the Ph.D. degree in software engineering from the College of Engineering, Florida Institute of Technology-Melbourne, USA, in 2002. He is currently an Associate Professor with the Software Engineering Department, College of Computer and Information Sciences (CCIS), King Saud University (KSU), Riyadh, Saudi Arabia, where he is also serving as the Vice Dean of the Research Chairs Program. He has authored or coauthored many publications. He has published over 70 research papers in the ISI-indexed journals of international repute. His research interests include software testing analysis and design, cloud computing, multimedia, the Internet of Things, big data, and mobile cloud. He has served as a Technical Program Committee Member of numerous reputed international conferences/workshops.

ATHANASIOS V. VASILAKOS is currently a Distinguished Professor with the Computer Science Department, Luleå University of Technology, Sweden. He has authored or coauthored over 250 technical papers in major international journals and conferences, five books, and 20 book chapters. His main research interests include cybersecurity, power systems cybersecurity, networking, the IoTs and smart cities, cloud computing, big data analytics, and machine learning.